Expert Systems With Applications 283 (2025) 127766

Contents lists available at ScienceDirect

Expert Systems With Applications

journal homepage: www.elsevier.com/locate/eswa

RegStack machine learning model for accurate prediction of tidal stream turbine performance and biofouling☆

Haroon Rashid [a], Mohd Hanzla [b], Tarek Berghout [c], Yassine Amirat [d], Arindam Banerjee [b], Abdeslam Mamoune [a], Mohamed Benbouzid [a,e,*]

[a] University of Brest, UMR CNRS 6027, 29238 Brest, France
[b] Department of Mechanical Engineering & Mechanics, Lehigh University, Bethlehem, PA 18015, USA
[c] University of Batna 2, Laboratory of Automation and Manufacturing Engineering, 05000 Batna, Algeria
[d] ISEN Yncrea Ouest, L@bISEN, 29200 Brest, France
[e] Shanghai Maritime University, Logistics Engineering College, 201306 Shanghai, China

ARTICLE INFO

Keywords:
Biofouling
Tidal stream turbine
Machine learning
Power coefficient
Thrust coefficient
Classification
RegStack algorithm

ABSTRACT

Tidal stream turbines (TSTs) are crucial for renewable energy generation but face challenges from marine biofouling, significantly impacting their efficiency. Traditional methods for predicting performance and detecting biofouling rely on empirical models and manual inspections, which are often time-consuming and less accurate. This study introduces RegStack, a novel machine learning-based ensemble model, to enhance the prediction of power and thrust coefficients (C_P and C_T) and accurately classify biofouling levels in TSTs. Unlike conventional models, RegStack integrates L1 and L2 regularization into a stacking framework, improving robustness, generalization, and interpretability. The model dynamically balances the strengths of multiple regression and classification algorithms, optimizing predictive accuracy while mitigating overfitting. Comprehensive experiments were conducted using an extensive dataset of tidal stream turbine performance metrics under varying operational and environmental conditions. The RegStack model outperformed conventional approaches, achieving a coefficient of determination (R^2) of 0.989 for performance predictions, with minimal mean absolute error (MAE) and mean squared error (MSE). Additionally, the model achieved 98.39% classification accuracy, with precision and recall of 0.97, and an F1-score of 0.97 in biofouling detection, demonstrating its effectiveness in real-time turbine health monitoring. By providing an automated, data-driven alternative to traditional methods, this study underscores the potential of advanced machine learning techniques in optimizing TST operations, reducing maintenance costs, and enhancing the reliability of marine renewable energy systems. The proposed RegStack model offers a scalable framework applicable to other renewable energy technologies, supporting sustainable energy advancements.

1. Introduction

1.1. Background

Tidal Stream Turbines (TSTs) are an innovative technology that harnesses the kinetic energy of tidal currents to generate electricity. These turbines operate similarly to underwater wind turbines, with rotor blades that are turned by the moving water, driving a generator to produce electricity. The basic components of a TST include the rotor blades, nacelle, and support structure (Touimi et al., 2018). The rotor blades are designed to efficiently capture energy from the water currents. As tidal currents flow over the blades, they spin, turning the generator within the nacelle to produce electricity (Liu et al., 2017). The support structure ensures the turbine is securely anchored to the seabed.

Tidal energy offers several advantages over other forms of renewable energy. Firstly, it is highly predictable, with tidal cycles being well understood and easily forecasted. This predictability enhances grid stability and makes tidal energy a dependable complement to more variable renewable sources like wind and solar (Liu et al., 2011; Rashid, Benbouzid, TitahBenbouzid, Amirat, Mamoune et al., 2023). Secondly,

☆ This work is supported by the PIA 3 CMQ Industries de la Mer Bretagne (IndMer), France.
* Corresponding author at: University of Brest, UMR CNRS 6027, 29238 Brest, France.
E-mail addresses: haroon.rashid@univ-brest.fr (H. Rashid), moh220@lehigh.edu (M. Hanzla), t.berghout@univ-batna2.dz (T. Berghout), yassine.amirat@isen-ouest.yncrea.fr (Y. Amirat), arb612@lehigh.edu (A. Banerjee), Abdeslam.Mamoune@univ-brest.fr (A. Mamoune), mohamed.benbouzid@univ-brest.fr (M. Benbouzid).

https://doi.org/10.1016/j.eswa.2025.127766
Received 29 January 2025; Received in revised form 7 April 2025; Accepted 14 April 2025
Available online 25 April 2025

TSTs have a lower visual impact and smaller footprint compared to wind farms, as they are installed underwater (Fox et al., 2018).

Tidal energy has a high energy density, meaning a small area of tidal turbines can produce a substantial amount of electricity (Gunawan et al., 2014). This efficiency, combined with the predictability of tidal flows, makes TSTs an attractive option for regions with strong tidal currents. By integrating tidal energy into the renewable energy portfolio, countries can diversify their energy sources, enhance energy security, and contribute to the reduction of greenhouse gas emissions (Ellabban et al., 2014).

The performance of TSTs is fundamentally assessed using two key parameters: the power coefficient (C_P) and the thrust coefficient (C_T). These coefficients are critical for evaluating the efficiency and operational dynamics of tidal turbines (Zhang et al., 2020).

The C_P is defined as the ratio of the actual power output of the turbine to the maximum power available in the tidal stream. Mathematically, it is expressed as:

$$C_P = \frac{Q\Omega}{0.5\rho A U^3} \tag{1}$$

where Q is the rotor torque, Ω is angular speed of the turbine, ρ is the density of seawater, A is the swept area of the turbine blades, and U is the velocity of the tidal stream. The C_P is a measure of the turbine's efficiency in converting the kinetic energy of the water into electrical energy. A higher C_P indicates better performance and efficiency of the turbine.

The C_T is defined as the ratio of the thrust force exerted on the turbine to the dynamic pressure force of the tidal stream. It is given by:

$$C_T = \frac{T}{0.5\rho A U^2} \tag{2}$$

where T is the thrust force. The C_T is significant because it quantifies the force exerted by the water on the turbine blades, which affects the structural load and stability of the turbine. Understanding C_T is crucial for designing turbines that can withstand the load they encounter during operation.

Both C_P and C_T are essential for optimizing the design and operation of TSTs. The C_P directly impacts the energy yield of the turbine, while the C_T influences the mechanical stresses and maintenance requirements. High C_T values can lead to increased wear and potential damage to the turbine structure, necessitating a balance between maximizing C_P and managing C_T (Volponi, 2014).

Monitoring and predicting these coefficients under various operational conditions, are vital for maintaining optimal performance of TSTs. Accurate prediction models enable better planning for maintenance and operational adjustments, ensuring the reliability of tidal energy systems (Arafat et al., 2024).

The TSTs are susceptible not only to severe hydrodynamic loading but also to the occurrence of biofouling on the TST blades and support structures (Hosna et al., 2023). Biofouling is the accumulation of marine organisms such as algae, barnacles, mussels, and other biological matter on submerged surfaces. This phenomenon occurs as microorganisms attach to surfaces in the water, forming a biofilm that attracts larger organisms over time. Biofouling is a significant challenge for marine renewable energy technologies, including TSTs, due to its impact on efficiency and maintenance. Walker et al. (2020) reported the growth of solid barnacles with heights of approximately 11 mm (0.02c, where c is the chord length), primarily on the trailing edge of the AHH HS1000 full-scale tidal turbine deployed at EMEC from December 2011 to early 2015. Similarly, biofouling accumulation has been reported for several other full-scale tidal turbines, including the Kobold tidal current turbine, the ducted axial-flow turbine at Canada's Race Rocks, and the OpenHydro TST (Rashid, Habbouche et al., 2024; Satrio et al., 2024).

Xu et al. (2025) proposed a multi-view and multi-type feature fusion (MVTFF) method for improved biofouling recognition on TST rotors. Their method enhances recognition accuracy by mitigating background interference and addressing target blending with water through the fusion of key boundary, semantic, and contour features. Experimental results demonstrated superior performance across varying water turbidity levels, improving mIoU, mPA, Precision, and Recall metrics. This approach contributes to optimizing TST maintenance and power generation efficiency. Fig. 1 shows the accumulation of biofouling on a tidal turbine after 28 days of installation.

A notable full-scale experimental investigation was conducted by SCHOTTEL HYDRO, where four drivetrains with 6.3-m rotors were deployed on the surface platform PLAT-I. The system underwent sea testing from 2017 to 2021 in Scotland and Nova Scotia, Canada. The study revealed that biofouling led to a significant power drop of up to 43% and a thrust reduction of 25%. These findings underscore the importance of maintaining turbine access for inspection and maintenance to mitigate performance degradation due to fouling (Rivier et al., 2018).

The process of biofouling begins with the initial colonization by bacteria and microalgae, which produce a slimy substance that facilitates the attachment of other organisms. Over time, this biofilm thickens and becomes a habitat for more complex organisms such as barnacles, mussels, and seaweed. The extent and type of biofouling can vary depending on environmental factors such as water temperature, salinity, and nutrient availability (Hong, Lv et al., 2024).

Biofouling has several adverse effects on the performance of TSTs:

- **Altered Hydrodynamic Characteristics:** Biofouling changes the hydrodynamic profile of turbine blades, affecting the lift-to-drag ratio. This alteration can compromise the optimal performance of the blades, further decreasing their ability to harness kinetic energy from tidal currents efficiently. The additional surface roughness disrupts the smooth flow of water over the blades, leading to increased resistance and decreased rotational speed. Consequently, the C_P drops, resulting in lower energy output.
- **Increased Structural Load:** The additional weight and surface area of biofouling organisms increase the standard deviation of the thrust force (C_T) exerted on the turbine blades. This heightened load can accelerate wear and tear on mechanical components, leading to more frequent maintenance and potentially shorter turbine lifespans.
- **Maintenance and Operational Costs:** Addressing biofouling involves regular cleaning and maintenance, which can be costly and time-consuming. Anti-fouling coatings and technologies add to the operational expenses but are necessary to mitigate the adverse effects of biofouling.

The impact of biofouling on TSTs underscores the importance of developing accurate predictive models for C_P and C_T under varying biofouling conditions. By understanding and anticipating the effects of biofouling, operators can implement more effective maintenance schedules and design strategies to enhance the efficiency of tidal energy systems. Based on the above studies, there is broad agreement within both the scientific community and the industry on the need to develop robust algorithms capable of predicting and detecting biofouling, enabling preventive maintenance. Most antifouling paints last for only 3–5 years, whereas these devices are designed for a lifespan of 20–30 years (Satrio et al., 2024).

The primary contributions of this study are as follows:

- Development of a novel hybrid model for turbine prediction, integrating ensemble learning techniques, feature selection optimization, and hybrid deep learning architectures.
- Introduction of a systematic approach to address data imbalance in turbine prediction.
- Demonstration of improved performance through the integration of L1 and L2 regularization.

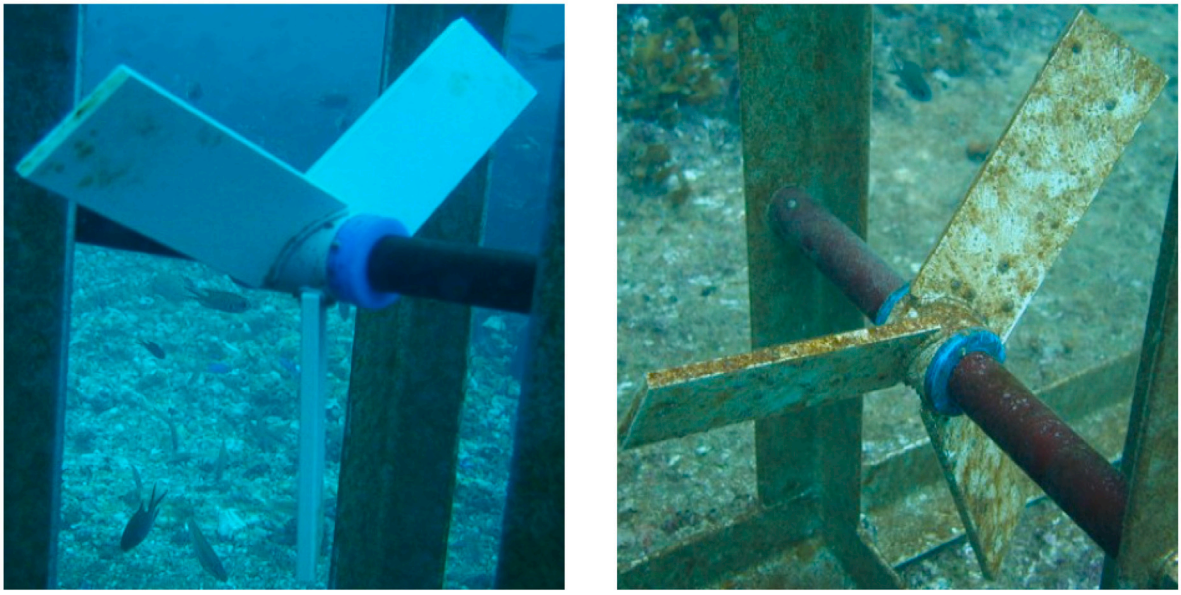

(a) After the installation (b) After one month of installation

Fig. 1. Biofouling accumulation on a tidal stream turbine.
Source: Courtesy of Prof. Kyozuka (2018).

- Classification models development based on bead distribution patterns on turbine blades to categorize turbine biofouling levels into distinct classes (clean, lightly fouled and densely fouled). This classification is crucial for effective maintenance planning and optimizing turbine operational performance.

2. Literature review

Turbine prediction methods can be broadly categorized into three main approaches:

Physics-Based Models: These models rely on fundamental fluid dynamics equations to predict turbine performance. Examples include Blade Element Momentum Theory (BEMT) and Computational Fluid Dynamics (CFD), which provide detailed flow analysis but require extensive computational resources and may struggle with real-time adaptability.

Data-Driven Models: These include machine learning (ML) and statistical models, such as Support Vector Machines (SVMs), Decision Trees, and DNNs. They excel at handling complex, nonlinear relationships but are prone to overfitting and require large, high-quality datasets.

Hybrid Approaches: These models combine physics-based and ML techniques to improve accuracy and adaptability.

A major challenge in turbine prediction is data imbalance, where most datasets are dominated by normal operating conditions, leading to biased models that fail to accurately predict rare failure events (Chen et al., 2024). Recent research suggests methods such as oversampling, cost-sensitive learning, and hybrid modeling to mitigate this issue (Chen et al., 2025, 2020). This study integrates these insights by developing a regularized ensemble learning approach that balances prediction accuracy while addressing data imbalance.

BEMT is one of the most widely used traditional computational models for predicting the performance of TSTs (Mannion et al., 2020; Masters et al., 2011). In Malki et al. (2013), the authors present an innovative hybrid modeling approach that integrates BEMT with Computational Fluid Dynamics (CFD) to enhance prediction accuracy. This method improves upon conventional BEMT by incorporating detailed flow analysis, making it more reliable for design optimization and operational strategies. However, purely physics-based models like BEMT and CFD require extensive computational resources and lack adaptability to dynamic environmental conditions, limiting their practical application in real-time performance monitoring.

Recent advancements have explored ML approaches as data-driven alternatives for predicting C_P and C_T. Various ML techniques, including SVMs, Decision Trees, and Deep Neural Networks (DNNs), have been employed to improve accuracy (Kishore et al., 2024; Yang et al., 2024). While these models outperform traditional computational methods in handling non-linearity, they often suffer from overfitting, interpretability challenges, and high sensitivity to dataset size. Furthermore, most existing ML models are designed exclusively for either performance prediction or biofouling classification, rather than integrating both tasks within a unified framework. Different machine learning models are summarized in Table 1, which provides a comparison of various machine learning techniques for performance analysis.

Traditional biofouling detection methods, such as visual inspection and periodic cleaning, are costly, time-consuming, and operationally disruptive (Hong, Deng et al., 2024; Rashid, Benbouzid, TitahBenbouzid, Amirat, Mamoune et al., 2023). Advanced sensor technologies have been introduced to address these challenges. Acoustic sensors, for example, use sound waves to detect and characterize biofouling based on changes in signal reflection (Kong et al., 2024). While effective, acoustic sensors are susceptible to environmental noise and require complex signal processing techniques to extract meaningful information.

Pretext tasks, such as contrastive learning and masked autoencoding, have emerged as powerful techniques in self-supervised learning for biofouling detection. These methods enable models to learn meaningful and robust feature representations from unlabeled data, addressing the challenge of limited annotated datasets (Prexl & Schmitt, 2025; Wang et al., 2024).

Optical imaging techniques, utilizing cameras, provide visual evidence of biofouling growth on turbine surfaces. These systems offer potential for automated image analysis but may be ineffective in turbid waters or environments with low optical clarity (Rashid, Benbouzid, Amirat et al., 2023). Recent studies have integrated ML-based image processing techniques to enhance biofouling classification accuracy. However, such methods still require extensive labeled datasets and suffer from domain adaptation issues when applied to different water conditions.

Table 1
Comparison of machine learning techniques for performance analysis.

ML technique	Key features	Advantages	Limitations	Reference
Artificial Neural Networks (ANNs)	Multi-layer perceptrons, non-linear modeling	High accuracy, good generalization	Requires large dataset, risk of overfitting	Rotor and Hefazi (2022)
Support Vector Regression (SVR)	Sensorless MPPT using the relationship between the generator's output power and rotational speed.	Avoids reliance on tidal current speed sensor, improves reliability, and reduces maintenance costs.	Performance influenced by parameter selection; requires offline training.	Abo-Khalil and Alghamdi (2021)
Random Forests (RF)	Ensemble of decision trees, feature importance	High accuracy, interpretable, handles missing data	Computationally expensive, may overfit with noisy data	Breiman (2001)
Gaussian Process Regression (GPR)	Probabilistic modeling, uncertainty quantification	Accurate predictions, provides confidence intervals	Computationally intensive, less effective with high-dimensional data	Banerjee et al. (2013)
Deep Learning (DL)	Convolutional neural networks, deep architectures	Superior accuracy, captures complex patterns	Requires large computational resources, risk of overfitting	Li et al. (2024)
Generative–Predictive Models	Data-driven multi-objective optimization, combines generative and predictive approaches	Capable of handling multiple objectives, high prediction accuracy	Complexity in model development and interpretation	Xia et al. (2024)
Statistical Models	Univariate Analysis, MDA, LPM	Simple interpretation, widely used	Limited for complex datasets	Mohanty et al. (2025)
Artificial Intelligence and Expert Systems	Inductive Learning, CBR, Neural Networks	Effective for decision making, adaptive	Computationally expensive, may require expert knowledge	Ducange et al. (2025) and Liu et al. (2025)

Mo et al. (2024) proposed a deep learning-based method for the identification of pollutant adhesion in tidal energy generation systems. Their approach utilizes underwater image datasets and image segmentation algorithms to accurately identify and quantify biofouling on turbine blades, significantly improving detection accuracy. These findings highlight the potential of machine learning in biofouling monitoring, further motivating the need for robust predictive models like RegStack.

Emerging trends in biofouling detection involve the use of machine learning for real-time anomaly detection. ML-driven approaches leverage sensor fusion techniques, combining acoustic, optical, and physical sensor data to enhance robustness (Rashid, Benbouzid, Titah-Benbouzid, Amirat, Berghout et al., 2023). Despite these advancements, most existing models focus on either predictive maintenance or biofouling classification, with limited research addressing an end-to-end framework for both tasks.

This study addresses the limitations of existing approaches by introducing RegStack, a novel stacking-based ensemble learning model that incorporates both L1 and L2 regularization within its meta-learner. Unlike conventional ML models, which focus solely on either C_P and C_T prediction or biofouling classification, RegStack provides a unified framework that effectively integrates both tasks. This comprehensive approach enhances predictive accuracy and operational efficiency in TST performance monitoring. Furthermore, RegStack improves model interpretability through SHAP-based feature importance analysis, mitigating the black-box nature of traditional ML techniques and offering deeper insights into the influence of key input variables.

3. Methodology

Fig. 2 outlines the general framework of the proposed methodology. The methodology involves several stages: Data collection, where raw data from TSTs is gathered; Data preprocessing, where the data is cleaned and prepared; Prediction of C_P and C_T using the proposed Regstack Method, leading to performance predictions; and Biofouling classification using the proposed Regstack Classifier to categorize the turbines as clean, lightly fouled, or densely fouled.

3.1. Data collection

3.1.1. Experimental facility

The experiments were conducted at the Tidal Turbulence Test Facility (T^3F) located at Lehigh University, Pennsylvania, USA, as shown in Fig. 3a. The water tunnel features an open surface test section with dimensions of 1.98 m in length (7.08D: D-turbine diameter), 0.61 m in width (2.18D), and water level depth is maintained at 0.60 m (2.14D) (Kolekar & Banerjee, 2015; Vinod & Banerjee, 2019; Vinod et al., 2021). The flow speed in the tunnel is maintained using a 25HP single-stage axial flow pump with a variable frequency driver. The facility can achieve a maximum of 1 m/s inflow speed. However, all the experiments conducted in this work were run at an inflow speed of 0.83 m/s.

A 1:20 scaled, three-bladed tidal turbine with a rotor diameter of 11″ (D = 0.279 m) and a constant chord c = 0.56″ (0.014 m) having SG6043 profiled blades was tested as shown in Fig. 3b. The turbine design is the same as used in previous studies (Habbouche et al., 2024; Kolekar et al., 2019; Modali et al., 2021; Rashid, Benbouzid et al., 2024; Vinod & Banerjee, 2019; Vinod et al., 2021) with a slightly shorter chord length. The rotor plane was fixed at 2D from the test section inlet with its axis along the tunnel centre line. An Anaheim Automation (23MDSI) stepper motor provided precise control of the rotor shaft's rotational speeds. The sensor assembly, located within the nacelle, included a torque (Interface Model-MRT2P) and thrust (SML-25) sensor to measure the loads on the rotor assembly. The nacelle having all the electronics is sealed with pressurized air around 20 kPa gauge pressure to prevent ingress of water inside it.

3.1.2. Measurement specifications

The thrust and torque data is sampled at 200 Hz sampling frequency for 120 s, which allows mean and standard deviations to converge with an error below 3% (see Fig. 2 in previous study (Vinod & Banerjee, 2019)). The non-repeatability of these sensors was ±0.0334 N and ±0.001 Nm, respectively. To minimize variability in the turbine data due to rotor degradation and supporting fixtures (shaft, bearings, coupling, stepper motor, to name a few), an initial dry (in-air) calibration of the torque and thrust sensors is performed. Subsequently, the experimental values obtained during actual testing are corrected accordingly. The accounted variability is less than ±3.25%, determined after repeating each experiment three times. The inflow velocity was measured using Nortek Vectrino+ Acoustic Doppler Velocimetry (ADV) sampled at 50 Hz sampling frequency. The measurement accuracy of the ADV provided by the manufacturer was ±0.005 m/s, and the data was collected for 120 s. The measured velocity time series is filtered using the phase space thresholding (PST) technique to eliminate spikes (Goring & Nikora, 2002). After filtering, the velocity time series is then decomposed using Reynolds decomposition into mean U and fluctuating $u'(t)$ components for further analysis.

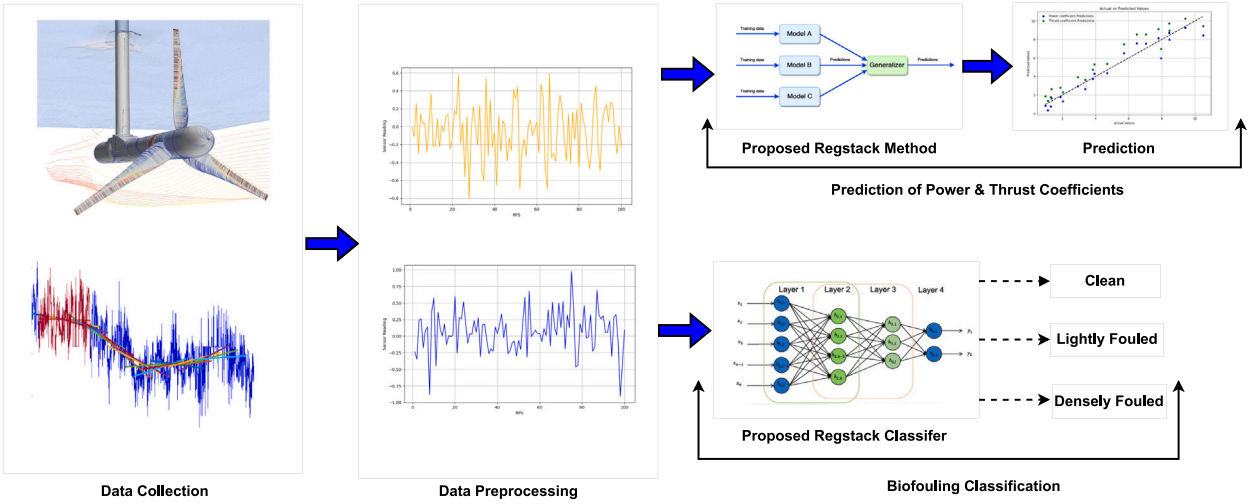

Fig. 2. General framework of the proposed methodology.

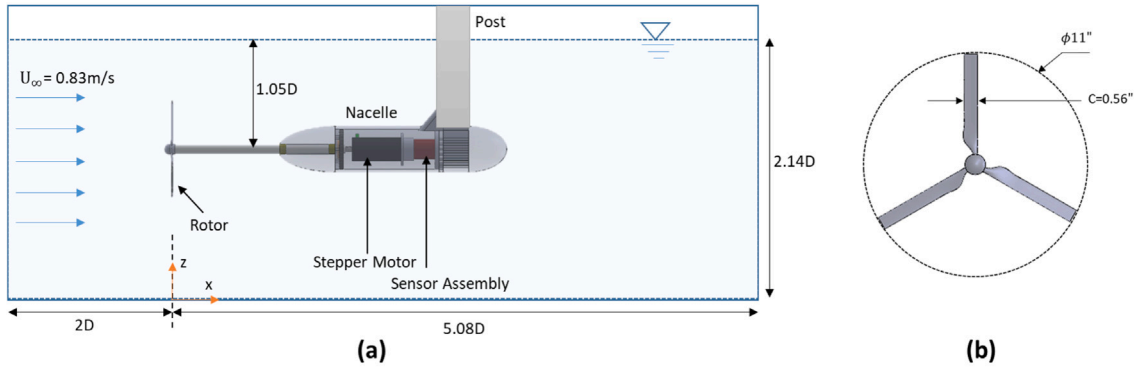

Fig. 3. (a) Schematic of Tidal Turbulence Test Facility (T^3F); (b) 1:20 scaled rotor used in the experiment.

3.1.3. *Inflow characterization*

Prior to the discussion on mimicking the effect of biofouling through roughness introduced by using beads, it would make more sense to elaborate on the inflow conditions. The current work uses a free-stream velocity of 0.83 m/s, which is quasi-laminar, i.e., having turbulence intensity (= $100x\sqrt{\overline{u'^2}}/U$; overbar represents time-average) at the center-point on the rotor plane around 2.2%. Similar values of freestream turbulence intensity in the same setup were reported in previous studies (Vinod & Banerjee, 2019; Vinod et al., 2021). Since the honeycomb mesh upstream of the test section can introduce variability due to ADV particle tracers getting trapped, it is regularly cleaned, and the tunnel is calibrated periodically to minimize any effects. Further, the generated inflow condition is homogeneous, as shown in the contour plots (Fig. 4a,b) for streamwise mean velocity and turbulence intensity (Ti%) at the rotor plane. The dashed line marks the trajectory of the blade tip shown only for the upper half-rotor plane. Clearly, a good homogeneity can be seen in the inflow condition, having variability in the mean velocity and turbulence intensity within ± 1.2% and ± 0.8%, respectively, at the rotor plane. Velocity spectra of the streamwise velocity time series data were also examined and plotted using Pwelch (MATLAB), as shown in (Fig. 4c). It can be seen that the velocity spectra do not have Kolmogorov -5/3 scaling and, hence, the inflow condition is not representative of the turbulent inflow (Pope, 2000) and can be regarded as quasi-laminar. The turbulence intensity reported is merely a measure of the background disturbances. This allows us to explicitly measure the effect of biofouling on the turbine performance with negligible interference from the free-stream turbulence.

The chosen free-stream velocity of 0.83 m/s is representative of the typical operational conditions in TST systems under moderate flow scenarios (Gunawan et al., 2014; Hanzla & Banerjee, 2025). Previous studies (Hanzla & Banerjee, 2025; Vinod & Banerjee, 2019; Vinod et al., 2021) found no further improvement in the scaled turbine performance by increasing mean velocity. Therefore, the present experimental campaign considered 0.83 m/s for all cases. It also falls within the operational range where the turbine blades can experience consistent performance without being dominated by extreme flow conditions. The present study with quasi-laminar inflow is designed to isolate any effect of freestream turbulence, and thus any attenuation in turbine performance is solely due to the biofouling effect. Further, the Reynolds number based on turbine diameter is 2.3 × 10 5, an order of magnitude lower than typical tidal sites (Gunawan et al., 2014) . Hence, the results are not claimed to be independent of the Reynolds number effect.

3.1.4. *Raw data for machine learning model*

The raw data used for developing the ML model includes measurements from sensors with specific attributes. The data collected includes measurements with an upper range value marked, and the measurements are adjusted using a moving average of 16 data points. This smoothing reduces the effects of high-frequency noise. The sampling rate of 200 Hz ensures that the measurements are collected frequently, which is beneficial for capturing dynamic (Hanzla & Banerjee, 2025). The accuracy class of 0.10% indicates that the measurement readings can vary by this amount from the true value. This level of uncertainty should be taken into account during the model development, as it affects the precision of the predictions.

- Sampling Rate: 200 samples per second ensures high temporal resolution, which is useful for detecting rapid changes or trends in the data.

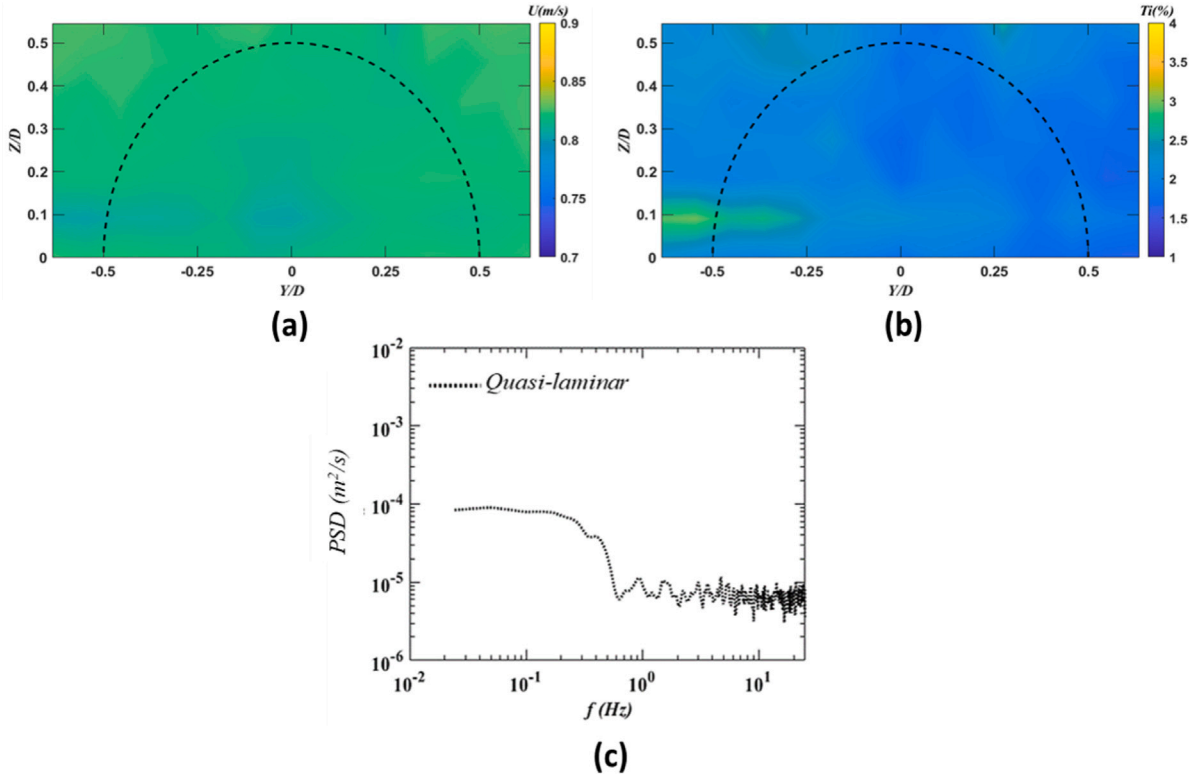

Fig. 4. Upper-half planar distribution of (a) streamwise mean velocity and (b) turbulence intensity (Ti%) at the rotor plane. (c) Power spectra (PSD) of the velocity at the center point.

- Averaging: The moving average filter (window size of 16) helps to reduce noise and stabilize the data, which is crucial for making reliable predictions in the ML model.
- Uncertainty: The 0.10% accuracy implies that the true values could differ from the sensor readings by up to 0.10%. This should be factored in when analyzing the data's reliability and when interpreting the ML model's outputs.

3.1.5. Data preprocessing

The dataset used in this study comprised approximately 24,000 datapoints collected across three cases: clean blades, lightly fouled blades, and densely fouled blades. These datapoints were generated from torque, thrust, and rotational speed measurements sampled at a high frequency of 200 Hz during each experimental run. This high-resolution sampling ensured the dataset captured the subtle variations in performance metrics caused by different biofouling conditions. The dataset was stored in a MySQL database, ensuring efficient retrieval and management. Data preprocessing involved an ETL pipeline using Python's Pandas and NumPy libraries. Outliers were detected and removed using the IQR method, and missing values were imputed using nearest-neighbor interpolation.

To prepare the data for machine learning, several preprocessing steps were undertaken. First, a phase-space thresholding technique was applied to detect and remove outliers, which are typically caused by sensor noise or environmental disturbances. This step was critical to maintain the integrity of the dataset and avoid skewing the model training process. Next, all input features, including torque, thrust, and rotational speed, were normalized using min–max scaling to a range of [0, 1]. This normalization ensured that all features contributed equally during model optimization and accelerated the convergence of the learning algorithm.

Derived features, such as tip-speed ratio (TSR) and non-dimensionalized coefficients for thrust and power, were computed to enhance the dataset's ability to represent turbine performance under different fouling conditions. Statistical descriptors such as mean, standard deviation, and skewness were also extracted from the time-series data to capture patterns that could indicate biofouling severity. To address class imbalance between clean, lightly fouled, and densely fouled cases, data augmentation was performed by generating synthetic datapoints within each class's parameter space, ensuring robustness in the classification task. Following these steps, the dataset was split into training, validation, and testing sets in a 70%:15%:15% ratio. The training set, consisting of approximately 16,800 datapoints, was used to train the RegStack model, while the validation and testing sets, each containing 3,600 datapoints, were employed for hyperparameter tuning and performance evaluation. Care was taken to ensure that all subsets preserved the distribution of clean and fouled cases to avoid introducing bias.

Additionally, missing data was addressed through linear interpolation or nearest-neighbor imputation to maintain a complete dataset without introducing noise. While dimensionality reduction through Principal Component Analysis (PCA) was explored as a potential step, the analysis confirmed that the selected primary features torque, thrust, and rotational speed captured most of the dataset's variance, validating their use in the final model. After completing these preprocessing steps, the final dataset included approximately 120,000 samples, enhanced with augmented data and derived features. These datapoints were used for training and evaluating the RegStack model, ensuring that the processed dataset was comprehensive, balanced, and ready for robust machine learning applications.

To ensure the robustness and interpretability of the RegStack model, we performed a comprehensive feature importance analysis using SHAP values. The input variables Torque (Channel A in Nm) and Thrust (Channel B in lbf), which are directly related to the C_P and C_T.

3.2. Data categorization

The dataset was categorized based on the application of plastic beads on the turbine blades to mimic hard biofouling conditions. Plastic

beads were used to simulate mature barnacle formations due to their controlled and reproducible geometry. The beads were selected based on their ability to mimic hard biofouling conditions effectively. However, it is acknowledged that this approach cannot fully replicate the variability in barnacle shape, size, and distribution seen in real-world scenarios. Future work will address this limitation by incorporating more complex and naturalistic biofouling models. Since biofouling (by barnacles, mussels, and other biological matter (Hosna et al., 2023; Kyozuka, 2018)) introduces an effect similar to enhanced surface roughness by tripping the fluid boundary layer (a condition similar to the issue of icing on wind turbine blades (Gao & Hu, 2021), the beads are a simple way to have a parametric study of biofouling. It is important to highlight that the beads have been used explicitly to mimic the mature barnacles, which are surface macrofouling. The barnacles can have a height that can exceed 10 mm (Barnes & Powell, 1950), which is generally much more than the boundary layer thickness formed on tidal turbine blades. A flow separation due to this surface roughness reduces the hydrodynamic lift while increasing the drag, thereby reducing the turbine power output. It is now well established that the height of surface roughness and its location play a significant role in the blade's hydrodynamic performance (Schultz et al., 2015; Stringer & Polagye, 2020; Walker et al., 2020). Since the present study is focused on detection and performance prediction due to biofouling. It is assumed that beads are well representative of the barnacles in this case. For simplicity, the barnacle/surface roughness height is limited, while the surface coverage varies only on the front surface of the blades. Table 2 summarizes the bead distribution on each of the three blades for two different cases considered, along with the clean blade as a baseline case. A brief discussion of each case is given below.

- **Clean blade**: This category represents blades without any beads applied, serving as the baseline or control condition (Fig. 5a).
- **Lightly fouled blades**: In this category, each of the three turbine blades has 8 plastic beads bonded randomly on their surface. This configuration is used to simulate a moderate level of surface roughness due to light biofouling (Fig. 5b). While the surface roughness at the leading edge has the most influence on blade performance and the least at the trailing edge (Stringer & Polagye, 2020), the random distribution allows no preference for barnacle colonization or its clustering. The random distribution is further motivated by the actual biofouling formed on the tidal turbine deployed for a month in Hirado Strait, Nagasaki (see Fig. 1b).
- **Densely fouled blades**: This category represents a higher level of surface roughness, where each of the three turbine blades has 17 plastic beads bonded randomly on their surface. This setup is used to simulate a more severe level of biofouling (Fig. 5c). Although, during turbine operation, it is more likely that the trailing edge is easily fouled (Walker et al., 2020), one cannot neglect the slack conditions and maintenance shutdowns when the turbine does not operate, and the entire blade surface can be easily fouled (Kyozuka, 2018).

The roughness length scale (l) is a parameter used to characterize the roughness of a surface. In the context of the turbine blades used in the experiment, this measure helps quantify the effect of the beads attached to the blades. According to Schultz et al. (2015), the roughness length scale can be calculated using the following formula:

$$l = 0.055k\sqrt{\%\text{coverage}} \tag{3}$$

where k is the height of the bead and % coverage is the percentage of the blade's surface area that is covered by the bead. This value is crucial because it directly influences the roughness length scale (Song et al., 2020). The higher the coverage percentage, the greater the impact of the roughness elements on the blade's hydrodynamic properties. Fig. 6 provide details of the beads used in the experiments. The diameter of the beads used is 0.237″ (6 mm) (see Fig. 6a), and

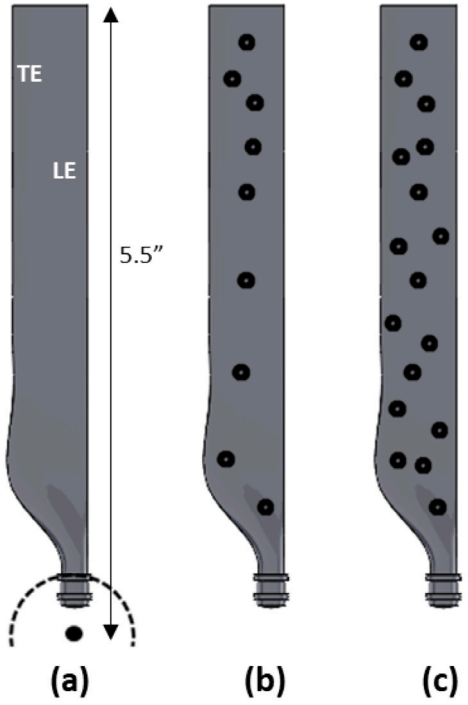

Fig. 5. Schematic of the beads and their distribution on the blade front face. (a) Clean; (b) Lightly fouled; (c) Densely fouled. LE — Leading Edge and TE — Trailing Edge of the blade.

the height/thickness is around 0.094″ (2.3 mm), as shown in Fig. 6b. Further, the k/c ratio is maintained at 0.16 (see Table 2), which is relatively much higher than previous studies having around 0.02 or lower (Farkas et al., 2022; Stringer & Polagye, 2020; Walker et al., 2014). The higher bead thickness is considered primarily when studying the mature barnacles, which could significantly affect the turbine performance. Previous studies (Stringer & Polagye, 2020; Walker et al., 2020) have shown actual barnacles of height around 1.5 mm could drop performance by 30%–50% while those of 4 mm can halt the turbine from producing any power. Vance and Fileman (2014) reported that dominant fouling barnacles at the EMEC Walls of Warness tidal site can reach heights of up to 30–40 mm in some cases. Therefore, we focus on the higher end of the k/c ratio, which mimics fully developed barnacles, representing an extreme operating condition. Subsequently, turbine performance is measured using embedded torque/thrust sensors at different tip speed ratios and compared with a clean blade under the same inflow conditions (quasi-laminar). The controlled variation of the tip speed ratio, ranging from 1 to 6, covers a broad operational range of tidal turbines (with full-scale turbines typically operating at TSR 3–4 (Harrold & Ouro, 2019). Furthermore, this study provides insights into how biofouling affects turbine performance under different operating conditions for a given distribution of fouling on the blade.

3.3. Machine learning techniques

3.3.1. Algorithm design

For the prediction of C_P and C_T, we employed a range of ML algorithms known for their effectiveness in handling complex datasets.

Random Forest Regressor: Random Forest is an ensemble learning method that constructs multiple decision trees during training and outputs the average prediction of the individual trees (Graw et al., 2021). It is effective for both regression and classification tasks, known for handling complex datasets and reducing overfitting.

Support Vector Regression (SVR): SVR is a variant of SVMs used for regression tasks. It finds a hyperplane in a high-dimensional space

Table 2
Details of bead distribution on turbine blades and its physical parameters.

Case name	Description	k/c ratio	Roughness length scale (mm)	Coverage (%)
Clean blade	No beads	–	–	–
Lightly fouled	All 3 blades having 8 beads distributed randomly	0.16	0.5000	14.5
Densely fouled	All 3 blades each having 17 beads distributed randomly	0.16	0.7108	29.3

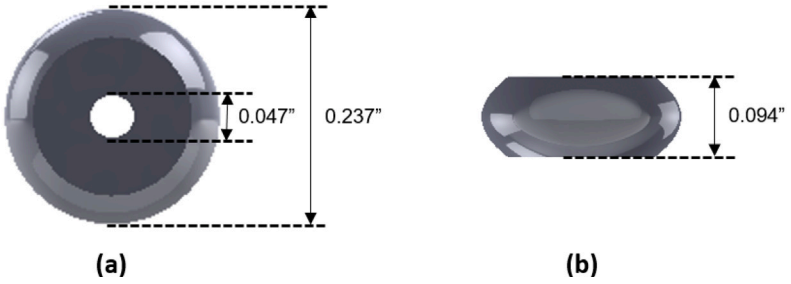

Fig. 6. Schematic of the bead. (a) Top view; (b) Side view.

that best fits the data points, aiming to minimize the error. SVR is suitable for predicting continuous values, especially in cases where the data has non-linear relationships and high dimensionality (Jiang et al., 2024).

Multi-layer Perceptron (MLP) Regressor: MLP Regressor is a type of artificial neural network (ANN) with multiple layers of neurons. Each neuron applies a weighted function to the input data and passes the result to the next layer. It is capable of capturing complex relationships in data and is particularly effective for tasks where non-linear patterns need to be modeled (Niu et al., 2024).

Gradient Boosting : Gradient Boosting is an ensemble technique where new models are sequentially added to correct the errors of previous models. It builds an ensemble of decision trees and optimizes them in a gradient descent manner (Zhu et al., 2024).

Voting Classifier: Voting Classifier combines multiple models (e.g., SVM, Random Forest, etc.) and predicts the class label by majority voting or averaging predicted probabilities. It improves the overall performance by aggregating predictions from different models, suitable when individual models complement each other (Khalid et al., 2024; Rashid, Benbouzid, Amirat et al., 2023).

3.3.2. Proposed RegStack method

This paper introduces RegStack, a novel regularized stacking regressor that combines L1 and L2 regularization to mitigate overfitting and enhance generalization, as illustrated in Fig. 7. Traditional stacking regressors often suffer from overfitting due to the complexity of the meta-learner. L1 regularization (Lasso) adds a penalty equal to the absolute value of the coefficients, promoting sparsity by pushing some coefficients to zero. L2 regularization (Ridge) adds a penalty equal to the square of the coefficients, preventing any coefficient from becoming too large. By integrating these regularizations into the meta-learner's objective function, RegStack improves robustness and accuracy.

The proposed RegStack method employs a two-stage optimization process. In the first stage, individual base models are trained on the dataset using different algorithms to ensure diversity in predictions. In the second stage, the meta-learner is trained by combining the predictions of the base models, incorporating L1 and L2 regularizations into its objective function. This dual-regularization approach allows RegStack to balance sparsity and stability in the coefficients, thereby mitigating overfitting while ensuring that no individual model dominates the final prediction. Extensive experiments demonstrate that RegStack consistently outperforms traditional stacking methods across multiple benchmark datasets, showcasing its ability to generalize well to unseen data.

The architecture of RegStack consists of multiple base models (such as decision trees, support vector regressors, and neural networks) whose outputs are combined by a meta-learner with elastic net regularization. The meta-learner is implemented using a linear model that integrates both L1 and L2 penalties. The training process begins with training the base models independently on the dataset. Their predictions are then fed into the meta-learner, which is trained using a loss function incorporating regularization. This process ensures that the model remains interpretable while improving generalization. The detailed architecture and training steps are visually summarized in Fig. 7.

The time complexity of the integrated model is primarily determined by two components: feature extraction and the ensemble model. The feature extraction step has a complexity of:

$$T_1(n) = O(n \log n) \tag{4}$$

where n is the number of data points, as it involves processing and transforming raw data into meaningful features. The ensemble model, which consists of multiple base models, requires:

$$T_2(n, m) = O(mn) \tag{5}$$

where m is the number of base models and n is the number of data points. Therefore, the overall time complexity of the model is given by:

$$T(n, m) = T_1(n) + T_2(n, m) = O(n \log n) + O(mn) \tag{6}$$

which ensures a balance between accuracy and computational efficiency, particularly when the number of base models is kept manageable.

To further enhance model performance, hyperparameter tuning was conducted to optimize the RegStack framework. We employed Grid Search to systematically explore a predefined set of hyperparameters and identify the best combination. Additionally, Bayesian Optimization was used to efficiently search the hyperparameter space by balancing exploration and exploitation. This ensured that the model achieved optimal regularization strengths for L1 and L2 penalties, maximizing predictive accuracy while minimizing overfitting.

Computational efficiency was also analyzed to assess the feasibility of deploying these models in real-time applications. The training time was measured for different models and compared against their predictive accuracy. While hyperparameter tuning introduced an initial computational overhead, it significantly improved model performance. The inference phase remained computationally efficient, demonstrating

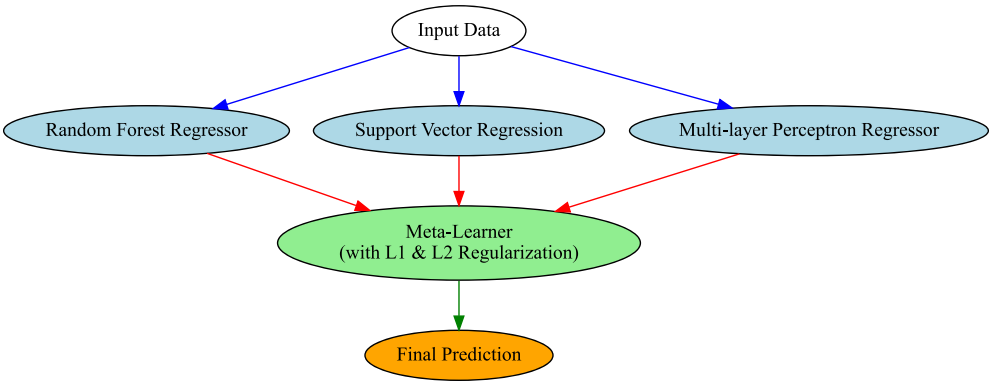

Fig. 7. Flow diagram of the proposed Regstack method.

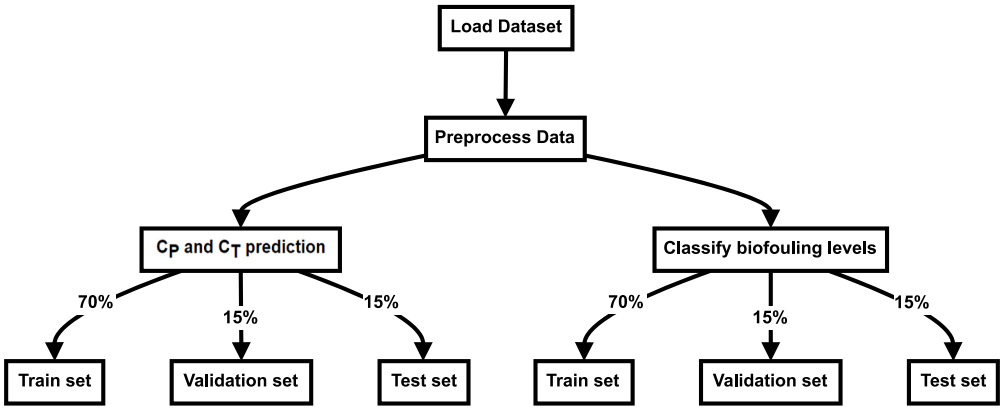

Fig. 8. Data distribution flowchart for machine learning.

the model's suitability for real-time prediction tasks in operational environments.

Although ensemble models like RegStack achieve high predictive accuracy, they can function as "black boxes", making it difficult to interpret their decision-making process. To improve transparency, this study incorporates SHAP (SHapley Additive Explanations) analysis, which quantifies the contribution of each input feature to the model's predictions. The results, as illustrated in Fig. 9, demonstrate that torque plays a dominant role in predicting performance coefficients, while thrust has a secondary influence.

3.3.3. Model training, validation, and testing

To predict the performance coefficients (C_P and C_T) of TST blades and classify their biofouling levels, model training, validation, and testing procedures were implemented as shown in Fig. 8. The dataset was initially loaded and preprocessed to extract relevant features such as torque, thrust, and RPS for regression tasks, and torque and thrust for classification purposes.

To predict the performance coefficients, the dataset was divided into three subsets: training, validation, and testing. Each model's performance was evaluated on the validation set using metrics such as Mean Absolute Error (MAE), Mean Squared Error (MSE), and score to assess predictive accuracy.

Similarly, for the biofouling classification task, the dataset was split into training, validation, and testing sets to maintain the distribution of biofouling classes ('Clean', 'Lightly Fouled', 'Densely Fouled'). Classification models were trained on the training set and evaluated on the validation set. The performance of each classifier was assessed based on accuracy and detailed classification metrics such as accuracy, precision, recall, and F1-score on the test set.

3.3.4. Model evaluation metrics

The analysis in this study is predominantly quantitative, relying on numerical evaluation metrics such as R^2, MAE, and classification accuracy to assess the model's performance. These metrics provide objective, measurable insights into the model's accuracy and prediction capabilities. However, a feature importance analysis is also conducted, which provides qualitative insights into the model's decision-making process, helping interpret how different input features influence predictions.

Mean Absolute Error (MAE):

Mean Absolute Error is the average of the absolute errors between the predicted values and the actual values. It gives an idea of how much the predictions deviate from the actual values, on average.

$$\text{MAE} = \frac{1}{n}\sum_{i=1}^{n}|y_i - \hat{y}_i| \tag{7}$$

where n is the number of observations, y_i is the actual value, and $\hat{y}_i$ is the predicted value.

Mean Squared Error: (MSE)

Mean Squared Error is the average of the squared errors between the predicted values and the actual values. It gives an idea of the variance of the prediction errors.

$$\text{MSE} = \frac{1}{n}\sum_{i=1}^{n}(y_i - \hat{y}_i)^2 \tag{8}$$

where n is the number of observations, y_i is the actual value, and $\hat{y}_i$ is the predicted value.

R^2 Score

The R^2 Score (Coefficient of Determination) is a statistical measure that represents the proportion of the variance for a dependent variable

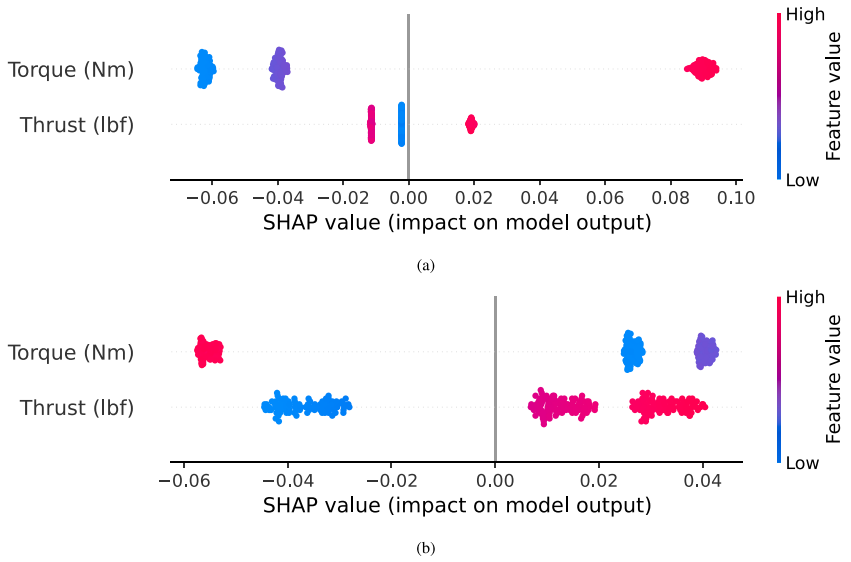

Fig. 9. Feature importance analysis using SHAP summary plots. (a) Contribution of features to C_P prediction. (b) Contribution of features to C_T prediction.

that is explained by an independent variable or variables in a regression model. It indicates the goodness of fit of the model.

$$R^2 = 1 - \frac{\sum_{i=1}^{n}(y_i - \hat{y}_i)^2}{\sum_{i=1}^{n}(y_i - \bar{y})^2} \tag{9}$$

where n is the number of observations, y_i is the actual value, $\hat{y}_i$ is the predicted value and $\bar{y}$ is mean of the actual values

4. Results

A comprehensive experimental analysis was conducted to validate the performance of the proposed approach. In addition to benchmarking RegStack against traditional methods, we also compared its performance with deep learning models.

4.1. Feature importance analysis

The feature importance analysis using SHAP values provides critical insights into the contributions of Torque (Nm) and Thrust (lbf) to the predictions of C_P and C_T. As illustrated in Fig. 9, the SHAP summary plots demonstrate the relative impact of these features.

Torque (Nm) is the most influential feature in predicting both C_P and C_T, as indicated by the wider distribution of SHAP values along the x-axis. Higher Torque values (red points) positively contribute to model predictions, while lower values (blue points) negatively impact them.

Thrust (lbf), although contributing to the predictions, has a noticeably smaller effect compared to Torque. The distribution of SHAP values for Thrust is narrower, confirming its relatively lower importance.

The color gradient in Fig. 9 further supports these findings, showing that increases in Torque generally result in higher C_P and C_T predictions. These results validate Torque as the primary driving factor in the model's predictions, while Thrust plays a secondary role.

4.2. Turbine performance coefficient

The performance and C_T of clean and fouled blades are first assessed based on the experimental measurements at different TSR. TSR is the non-dimensionalized parameter relating the blade tip speed to the inflow speed and is defined as:

$$TSR = \frac{\Omega D}{2U} \tag{10}$$

Since the experimental setup offers a blockage of around 16.5%, the performance data (C_P, C_T, and TSR) is corrected for blockage using the technique outlined in Bahaj et al. (2007), and as done in previous studies (Vinod & Banerjee, 2019; Vinod et al., 2021). Fig. 10a shows the C_P variation with TSR up to 6. The clean blade has the highest C_P values, with maxima between TSR of 4.5–5, confirming the previous findings in the same setup (Vinod & Banerjee, 2019). With increasing coverage of fouling (i.e., beads), the performance drops significantly. A drop of around 35% was found in maximum C_P for lightly fouled cases, which further increases with densely fouled blades. Similar findings of drop in turbine performance were also reported in previous studies (Farkas et al., 2022; Song et al., 2020; Stringer & Polagye, 2020) ranging from 12% to 50% and higher. The higher drop in our lightly fouled blades is primarily because of the beads' height (k/c = 0.16). Previous studies (Schultz et al., 2015; Song et al., 2020; Stringer & Polagye, 2020) have shown that the higher the roughness height, the more the maximum performance coefficient drops. Although the performance degradation with barnacles is intuitive, the current study shows that beyond a certain k/c ratio and %coverage, the turbine can no longer be considered a power-generating device. This is explicitly shown with densely fouled blades, which have negative C_P values, i.e., the turbine ceases to generate power. Fig. 10a also shows the possibility of shifting in the optimal TSR with increased fouling, similar to the results shown in (Stringer & Polagye, 2020). It is important to mention that the results shown in the current study are at Reynolds number $Re_D = 2.3 \times 10^5$, and in no way claimed to be Re independent.

Apart from the turbine performance, the C_T also drops with increased fouling at all TSR, as shown in Fig. 10b. The drop is significantly higher for TSR < 4 (up to 40%) while it reduces to ≃12% at the highest TSR. These results are in accordance with the previous studies done with axial or cross-flow turbines (Song et al., 2020; Stringer & Polagye, 2020). The C_T values for both the fouled cases do not show such differences as in the case of C_P. Further, the presence of fouling can also increase the load fluctuations on the rotor, as depicted in Figs. 10c,d. An increase of nearly 4.8 times in C_P and 2.0 times in C_T values compared to the clean blade was observed at the highest TSR for the fouled cases. Although fouling would likely reduce the mean thrust load, the increase in load fluctuations could significantly affect the fatigue life of the blades along with the performance degradation. This would further escalate in the presence of elevated turbulence observed in tidal sites (Thomson et al., 2012; Vinod & Banerjee, 2019), which is not considered in the present study. Therefore, it would be highly beneficial to have models that can accurately predict and detect biofouling on the tidal turbine blades, allowing preventive maintenance.

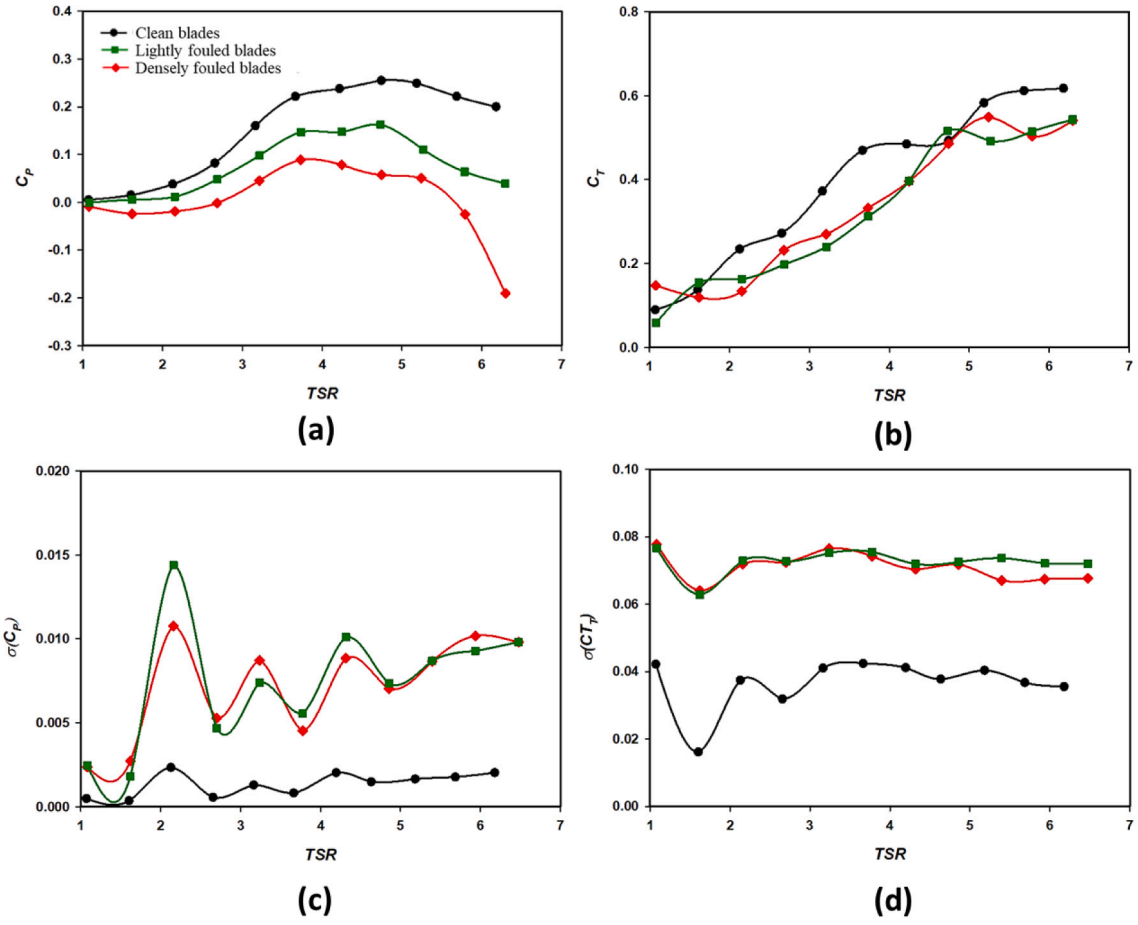

Fig. 10. (a) Turbine C_P, (b) C_T, and corresponding standard deviation values in (c) and (d), respectively. Values are plotted at different TSR for the three cases considered.

4.3. Model performance

Table 3 presents the prediction performance of various ML models for C_P and C_T. The proposed RegStack model achieved the highest performance across all metrics, indicating exceptional predictive accuracy. The Gradient Boosting Regressor also performed well, demonstrating strong prediction capabilities. The MLP Regressor had good accuracy but was slightly outperformed by the other models. The Voting Regressor showed moderate performance, while the Support Vector Regressor (SVR) had the lowest prediction accuracy among the models evaluated.

A comparative analysis of deep learning algorithms such as RNN, LSTM, CNN, DBN, and AE is shown in Table 3, where the RNN, LSTM, CNN, DBN, and AE models were evaluated alongside the traditional machine learning models. The results highlight that while these DL models showed improved performance compared to simpler models like SVR and Least-Squares Fitting, they still did not surpass the performance of the proposed RegStack model in terms of predictive accuracy. Specifically, the LSTM model showed the highest performance among the DL algorithms, but RegStack outperformed all models, including the deep learning approaches.

Additionally, the performance of simpler models such as least squares fitting and polynomial regression (degree 2) was also evaluated. Least-squares fitting showed a higher MAE and MSE compared to the ML models, and its R^2 value was considerably lower, indicating a reduced accuracy. Polynomial regression (degree 2) performed better but still lagged behind the other more complex machine learning models. These results highlight the advantage of using more sophisticated models, such as RegStack, which significantly outperforms these traditional methods in terms of predictive accuracy and robustness.

Table 3
C_P and C_T prediction performance of various machine learning models.

Model	MAE	MSE	R^2
SVR	0.0423862	0.00260281	0.643
MLP Regressor	0.00166189	4.34486×10^{-6}	0.963
Gradient Boosting Regressor	0.000347702	2.41080×10^{-7}	0.976
Voting Regressor	0.0207473	0.000634718	0.913
RNN	0.00512	1.02×10^{-5}	0.920
LSTM	0.00431	8.15×10^{-6}	0.934
CNN	0.00645	1.24×10^{-5}	0.901
DBN	0.00803	2.01×10^{-5}	0.852
AE	0.00722	1.83×10^{-5}	0.873
Least-Squares Fitting	0.0357321	0.00189203	0.720
Polynomial Regression (degree 2)	0.0212137	0.00054901	0.841
RegStack (proposed)	1.40847×10^{-5}	1.35406×10^{-9}	**0.989**

To validate the effectiveness of integrating L1 and L2 regularization, we conduct an ablation study with three configurations: (1) L1-only regularization, (2) L2-only regularization, and (3) Combined L1 and L2. The results, presented in Table 4, show that the combined approach yields the lowest prediction error and highest generalization ability.

4.4. Prediction of power and thrust coefficients

Figs. 11 and 12 depict the graphical representation of model performance, generated using Matplotlib and Seaborn libraries. Fig. 11 shows three scatter plots that illustrate the performance of three different

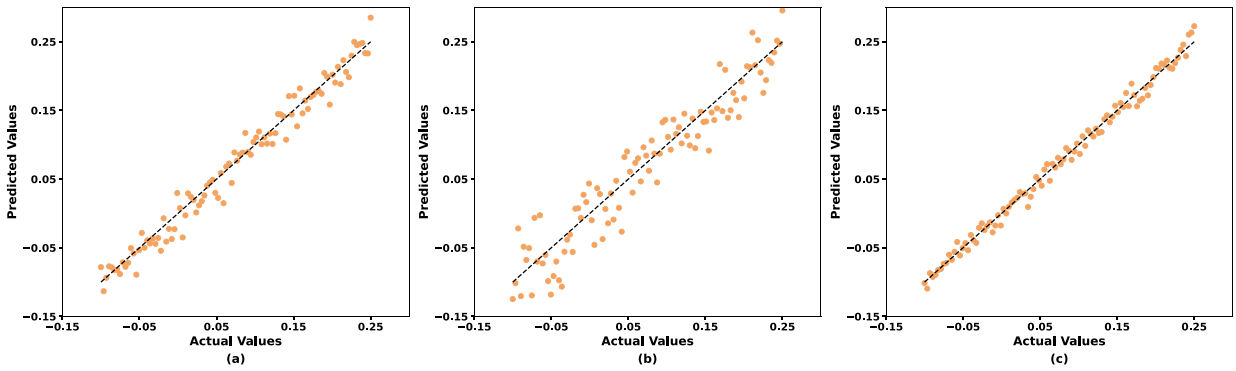

Fig. 11. Comparison of the predicted values to the actual values of C_P and C_T. (a) SVR; (b) Voting regressor; (c) Proposed Regstack.

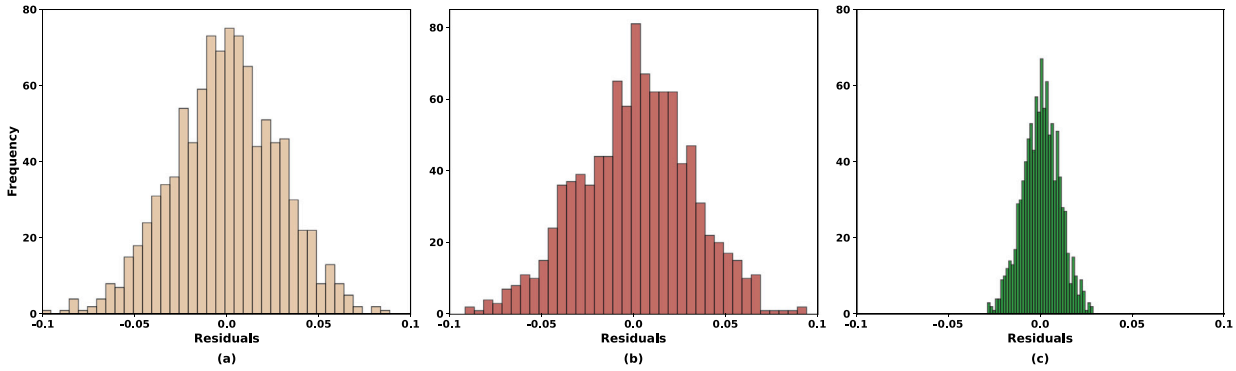

Fig. 12. Residual distributions of three different regression models. (a) SVR; (b) Voting regressor; (c) Proposed Regstack.

Table 4
Ablation study results for L1 and L2 regularization.

Model configuration	Accuracy (%)	RMSE	F1-score
L1 regularization	87.5	0.45	0.82
L2 regularization	88.2	0.42	0.84
L1 + L2 regularization	90.1	0.38	0.88

ensemble regression models. Each plot shows actual values on the x-axis with predicted values on the y-axis, with the black dashed line representing perfect predictions. In Fig. 11(a), the SVR's predictions are somewhat close to the diagonal line but show a fair amount of spread, indicating that while it can capture trends, it has noticeable prediction errors. Fig. 11(b), representing the Voting Regressor, shows a more dispersed scatter of points, indicating less accuracy and a wider spread of prediction errors. This suggests potential overfitting or insufficient tuning of the combined models. In contrast, Fig. 11(c), showcasing the proposed Regstack Regressor, reveals points tightly clustered along the diagonal line, reflecting strong alignment between predicted and actual values. This tight clustering signifies high predictive accuracy, demonstrating that the Regstack Regressor effectively captures the data's relationships and provides reliable predictions.

In Fig. 12, the residual distributions of three different regression models are illustrated.

Fig. 12a shows the residual distribution for the SVR. The residuals are widely dispersed across the range, with significant frequencies on both the positive and negative sides. This wide distribution indicates that the SVR has higher variability in its prediction errors, reflecting lower accuracy. The presence of many large residuals suggests that this model struggles to predict accurately for many instances.

Fig. 12b presents the residual distribution for the Voting Regressor. The residuals are somewhat more concentrated around zero compared to the SVR, but there is still a notable spread. The Voting Regressor shows an improvement over the SVR, with more predictions closer to the actual values. However, the considerable spread indicates that while the Voting Regressor is better, it still has room for improvement in reducing prediction errors.

Fig. 12c depicts the residual distribution for the proposed Regstack Regressor. The residuals are highly concentrated around zero, with very few residuals deviating far from zero. This tight distribution indicates high precision and accuracy in its predictions. The concentration of residuals around zero suggests that the Regstack Regressor makes very accurate predictions with minimal error, outperforming both the SVR and the Voting Regressor.

4.5. Classification of turbine biofouling levels

Table 5 shows the classification performance of three models used to predict biofouling levels on TST blades. The Gradient Boosting Classifier achieves an accuracy of 96.39%, with precision, recall, and F1-score values of 0.94, 0.95, and 0.94, respectively, indicating robust performance in identifying both positive and negative instances. In comparison, the Voting Classifier achieves an accuracy of 85.62% with consistent precision, recall, and F1-score metrics of 0.86, demonstrating reliable but slightly lower performance than the Gradient Boosting Classifier. The proposed RegStack model demonstrated superior classification accuracy (98.39%) and significantly reduced misclassification rates compared to conventional ML approaches. Real-time data adaptability further validates its applicability in operational environments and precision, recall, and F1-score metrics all at 0.97, highlighting its effectiveness in accurately classifying biofouling levels. These results suggest that the proposed RegStack Classifier is the most suitable model for this classification task due to its superior performance metrics.

Fig. 13 provides a comprehensive understanding of the performance of biofouling classification. The proposed RegStack Classifier consistently outperforms the other models across all classes in terms of precision, recall, and F1-score. The Gradient Boosting model also performs well, particularly for the clean and densely fouled classes. The

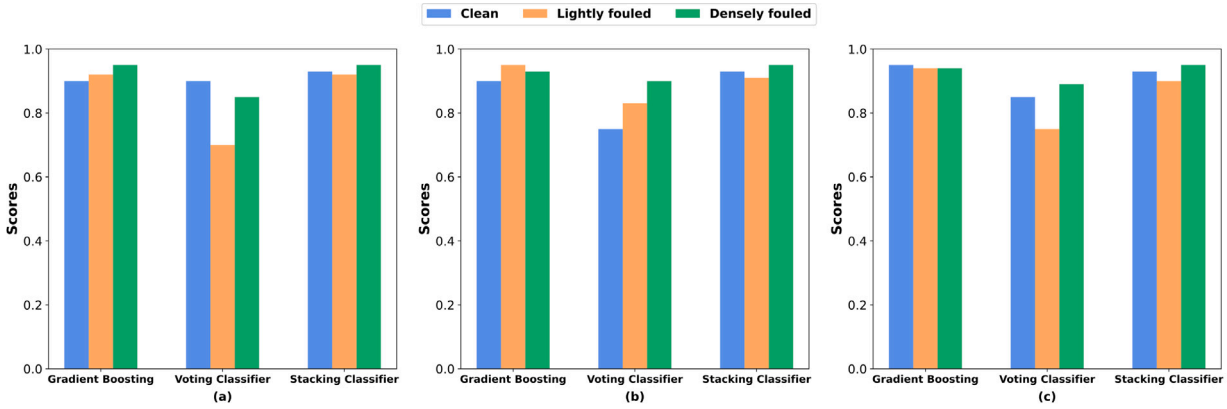

Fig. 13. Performance metrics for three classification models used to predict biofouling levels on tidal stream turbine blades. (a) Precision; (b) Recall; (c) F1 Score.

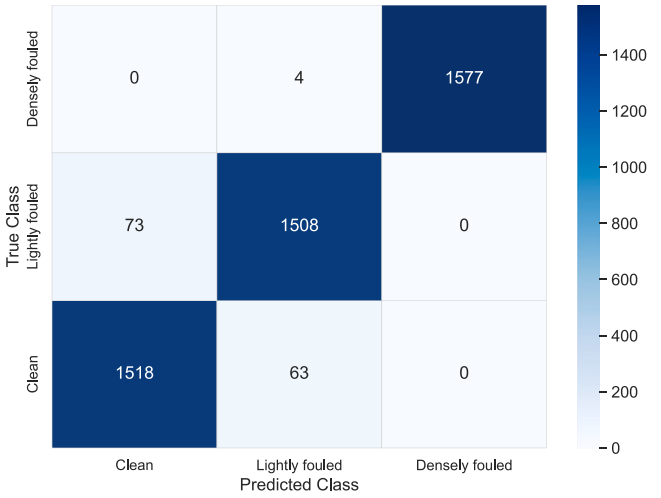

Fig. 14. Confusion matrix of the proposed RegStack classifier for classification of biofouling.

Table 5
Comparison of machine learning models for biofouling classification.

Model	Accuracy (%)	Precision	Recall	F1-score
Gradient Boosting Classifier	96.14	0.94	0.95	0.94
Voting Classifier	85.62	0.86	0.86	0.86
RegStack (proposed)	**98.39**	**0.97**	**0.97**	**0.97**

Voting Classifier shows lower precision and F1-scores, particularly for the lightly fouled class, indicating that it is less effective at correctly identifying instances in this category.

Fig. 14 displays the confusion matrix obtained from the evaluation of the proposed RegStack classifier for biofouling classification. The matrix summarizes the model's predictive performance across three classes: clean, lightly fouled, and densely fouled.

5. Discussion

5.1. Results analysis

The results from our experiments highlight the effectiveness of various ML models in predicting the C_P and C_T of TST, as well as classifying biofouling levels in the blades of turbines. Among the models tested, the proposed RegStack model demonstrated exceptional predictive accuracy, achieving the highest performance across all metrics, including MAE, MSE, and R^2 scores. This indicates that RegStack is highly capable of capturing the complex relationships in the data without overfitting.

The impact of biofouling on the C_P and C_T was evident from the classification results. The high accuracy of the RegStack Classifier (98.39%) in predicting biofouling levels suggests that biofouling significantly affects turbine performance metrics. Models with lower prediction accuracy for C_P and C_T, such as SVR and Voting Regressor, showed a reduced ability to capture the impact of biofouling, further emphasizing the sensitivity of turbine performance to biofouling conditions.

CNNs, while effective for biofouling detection, face computational bottlenecks such as high memory usage, long training times, and inference latency. These challenges can be mitigated by ensemble methods like RegStack, which combine multiple models to improve performance while offering a trade-off between computational complexity and accuracy. RegStack can potentially reduce the need for excessively deep networks, balancing model efficiency with detection accuracy.

5.2. Comparison analysis

Traditional methods for predicting turbine performance and assessing biofouling often rely on empirical formulas and manual inspections, which can be time-consuming and less accurate (Rashid, Benbouzid, TitahBenbouzid, Amirat, Mamoune et al., 2023; Rashid, Habbouche et al., 2024). RegStack's scalability for multi-objective tasks, such as balancing energy yield with structural load, highlights its versatility in optimizing competing objectives. By combining multiple models, RegStack can efficiently navigate trade-offs between different performance metrics, providing a flexible solution for complex optimization problems where both efficiency and robustness are required. This adaptability makes it particularly suitable for applications where multiple objectives need to be simultaneously optimized.

The ML approach provides several advantages over traditional methods:

- **Accuracy:** The RegStack model significantly outperformed traditional models, capturing the intricate patterns in the data.
- **Efficiency:** ML models can process large datasets quickly and update predictions in real-time, offering significant time savings over manual methods.
- **Adaptability:** These models can adapt to new data and evolving patterns, improving their predictive capabilities over time.

However, there are also some limitations to consider:

- **Data Dependency:** The performance of ML models is highly dependent on the quality and quantity of the training data.
- **Complexity:** Implementing and fine-tuning ML models requires specialized knowledge and computational resources.

- **Interpretability:** Some ML models, particularly ensemble methods like Gradient Boosting, can act as black boxes, making it challenging to interpret the underlying decision-making process.

While the RegStack model demonstrates high accuracy in predicting turbine performance and biofouling classification, it requires significant computational resources for both training and deployment. This could present challenges in real-time applications, especially in resource-constrained environments such as offshore monitoring stations with limited processing capabilities. Future work can explore model optimization techniques such as pruning and quantization to reduce the model size and improve inference speed. Furthermore, edge computing approaches, where computations are performed on-site using optimized embedded systems, can significantly reduce latency and reliance on cloud-based processing. These enhancements will make RegStack more practical for real-time turbine health monitoring and biofouling detection in operational settings.

5.3. Practical implications

The insights gained from this study have several practical implications for turbine maintenance and efficiency improvement:

- **Computer-Aided Detection (CAD) system:** The proposed RegStack model serves as a CAD system for turbine monitoring. Its real-time prediction capabilities facilitate early biofouling detection, reducing maintenance costs and improving efficiency.
- **Maintenance Scheduling:** Accurate prediction of C_P and C_T, along with reliable classification of biofouling levels, enables more efficient maintenance scheduling. Operators can prioritize cleaning and repairs based on the severity of biofouling, reducing downtime and extending the operational life of turbines.
- **Efficiency Improvement:** By understanding the impact of biofouling on turbine performance, operators can optimize the design and operation of turbines to minimize the adverse effects of biofouling, thereby improving overall energy conversion efficiency.
- **Real-Time Monitoring:** The ML models developed in this study have the potential to be integrated into real-time monitoring systems. Such systems could provide continuous assessment of turbine performance and biofouling levels, enabling automated responses to mitigate the effects of biofouling.
- **Automated Detection:** The high accuracy of the classification models suggests that automated detection of biofouling is feasible. Implementing such systems can reduce the need for manual inspections, thereby lowering operational costs and enhancing safety.

5.4. Applicability and limitations of the proposed approach

The RegStack model demonstrated exceptional accuracy for the specific dataset used in this study, making it highly applicable to scenarios involving controlled experimental conditions. Its ability to classify biofouling levels and predict C_P and C_T highlights its potential for integration into operational frameworks for TSTs. The present study is the first attempt to validate the model in a clean and controlled environment to assess its accuracy in biofouling detection and prediction. We have ensured that the flow remains free from environmental effects such as variability, turbulence, and shear, among others, so that turbine performance is solely influenced by fouling (plastic beads) on the blades. Previous work has also shown that turbine performance degrades in the presence of turbulence and shear (Vinod et al., 2021). Therefore, the model validation in this study is conducted under quasi-laminar inflow conditions to exclude such effects. The versatility of the model in addressing biofouling detection and its predictive capabilities provide a solid foundation for operational deployment, allowing for the optimization of turbine maintenance strategies and performance monitoring in a variety of settings. Additionally, the modular structure of the ML pipeline allows for extensions to other turbine designs, provided sufficient domain-specific data is available. This adaptability positions the RegStack model as a valuable tool for future studies and industrial applications.

However, there are several limitations that need to be addressed. Deep learning models often suffer from overfitting and require large datasets for effective training. The complexity of hyperparameter tuning and the need for computational resources pose additional challenges. The dataset was generated under controlled laboratory conditions, which may not encompass the variability encountered in real-world scenarios, such as extreme environmental conditions or diverse biofouling patterns. Extending the dataset to include real-world data will enhance the model's robustness.

The model's performance has been validated using a specific turbine design and flow conditions. Although the turbine is a 1:20 scale model with a specific SG6043 hydrofoil, the performance trends observed in our experiments are consistent with those reported for other turbine designs and scales in previous studies (Bachant & Wosnik, 2016; Bahaj et al., 2007; Harrold & Ouro, 2019; Perez et al., 2022). Therefore, we believe the model should be applicable to other turbine designs and scales as well. However, additional validation and generalizing the findings to other turbine geometries, larger scales, or untested operational settings will require retraining or fine-tuning the model with additional data.

Real-world environments introduce complexities such as fluctuating flow conditions, dynamic marine ecosystems, and sensor inconsistencies, which may impact model performance. A key limitation of this study is the reliance on controlled experimental data, which may not fully capture the variability of real-world turbine operations. Factors such as fluctuating marine conditions, seasonal biofouling variations, and sensor inaccuracies could influence model performance. Additionally, while the proposed model demonstrates high accuracy, its computational feasibility for real-time applications remains to be explored. Future work should focus on incorporating diverse field data, assessing model adaptability to different turbine configurations, and integrating explainable AI techniques to enhance interpretability and operator trust. Moreover, the robustness of the model to adversarial data shifts and sensor noise, common in real-world environments, should be examined. These factors could significantly affect model performance and generalizability, requiring the development of techniques to mitigate their impact. Further, future studies should also account for the diversity and variability of natural biofouling (e.g., algae, mussels). In fact, these diverse forms of biofouling could also lead to substantial reductions in turbine performance (Starzmann et al., 2022).

By addressing these aspects, the proposed model can transition from lab-based validation to real-world deployment, ensuring its effectiveness in optimizing TST performance and biofouling management.

6. Conclusions

This study introduces RegStack, a novel ensemble learning approach, to significantly enhance the prediction of C_P and C_T and accurately classify biofouling levels in tidal stream turbines (TSTs). Unlike conventional empirical and physics-based models, RegStack incorporates L1 and L2 regularization within a stacking framework, effectively balancing model complexity and generalization. This innovation mitigates overfitting while improving interpretability, marking a key advancement in machine learning applications for renewable energy systems.

Extensive experiments demonstrate that RegStack consistently outperforms conventional approaches, achieving a coefficient of determination (R^2) of 0.989 for turbine performance predictions and 98.39% classification accuracy in biofouling detection, with an F1-score of 0.97. These results highlight RegStack's ability to capture complex

nonlinear relationships between turbine performance metrics and operational conditions, improving the accuracy and efficiency of predictive modeling.

This work advances the state of knowledge by addressing key limitations of traditional methods, such as their reliance on empirical formulas and manual inspections, which are often less accurate and time-intensive. The RegStack model provides a data-driven, automated alternative capable of adapting to real-world variations in turbine performance and biofouling dynamics.

Beyond its immediate application to TSTs, the proposed RegStack framework can be extended to other renewable energy technologies, such as wind turbines, where performance degradation due to environmental factors remains a significant challenge. This scalability makes RegStack a promising tool for improving predictive maintenance strategies, reducing operational costs, and enhancing the long-term reliability of renewable energy infrastructure.

Future research should focus on further enhancing the model's generalizability by incorporating a broader range of environmental conditions and turbine configurations. Additionally, integrating RegStack into real-time monitoring systems can facilitate continuous performance assessment and proactive biofouling mitigation, paving the way for fully autonomous, self-optimizing renewable energy systems. Future work can also explore model optimization techniques such as pruning and quantization to reduce the model size and improve inference speed. Additionally, leveraging hardware acceleration through Graphics Processing Units (GPUs) or Tensor Processing Units (TPUs) can enhance computational efficiency.

By advancing predictive capabilities, operational efficiency, and automated maintenance strategies, this study makes a substantial contribution to the development of sustainable and reliable marine renewable energy solutions.

CRediT authorship contribution statement

Haroon Rashid: Conceptualization, Data curation, Formal analysis, Investigation, Methodology, Software, Validation, Visualization, Writing – original draft. **Mohd Hanzla:** Data curation, Investigation, Writing – review & editing. **Tarek Berghout:** Methodology, Writing – review & editing. **Yassine Amirat:** Formal analysis, Methodology, Validation, Visualization, Writing – review & editing. **Arindam Banerjee:** Methodology, Writing – review & editing. **Abdeslam Mamoune:** Funding acquisition, Supervision, Validation, Visualization, Writing – review & editing. **Mohamed Benbouzid:** Conceptualization, Funding acquisition, Formal analysis, Project administration, Methodology, Supervision, Validation, Visualization, Writing – review & editing.

Declaration of competing interest

The authors declare that they have no known competing financial interests or personal relationships that could have appeared to influence the work reported in this paper.

Acknowledgments

The authors would like to thank the Collège Doctoral de Bretagne (ED SPI.bzh) and the University of Brest, France for their support for the international mobility of Haroon Rashid to Lehigh University (USA). The authors also would like to thank Cong Han, Ph.D. student at Lehigh University, for his assistance in capturing the images used for this study. Arindam Banerjee would also like to acknowledge funding support by the US Department of Energy, Office of Energy Efficiency and Renewable Energy (EERE), specifically the Water Power Technology Office under award number DE-EE0009450.

Data availability

Data will be made available on request.

References

Abo-Khalil, A. G., & Alghamdi, A. S. (2021). MPPT of permanent magnet synchronous generator in tidal energy systems using support vector regression. *Sustainability*, *13*(4), 2223.

Arafat, M., Hossain, M., & Alam, M. M. (2024). Machine learning scopes on microgrid predictive maintenance: Potential frameworks, challenges, and prospects. *Renewable and Sustainable Energy Reviews*, *190*, Article 114088.

Bachant, P., & Wosnik, M. (2016). Effects of Reynolds number on the energy conversion and near-wake dynamics of a high solidity vertical-axis cross-flow turbine. *Energies*, *9*(2), 73.

Bahaj, A., Molland, A., Chaplin, J., & Batten, W. (2007). Power and thrust measurements of marine current turbines under various hydrodynamic flow conditions in a cavitation tunnel and a towing tank. *Renewable Energy*, *32*(3), 407–426.

Banerjee, A., Dunson, D. B., & Tokdar, S. T. (2013). Efficient Gaussian process regression for large datasets. *Biometrika*, *100*(1), 75–89.

Barnes, H., & Powell, H. T. (1950). The development, general morphology and subsequent elimination of barnacle populations, balanus crenatus and b. Balanoides, after a heavy initial settlement. *Journal of Animal Ecology*, *19*(2), 175–179.

Breiman, L. (2001). Random forests. *Machine Learning*, *45*, 5–32.

Chen, W., Yang, K., Yu, Z., Nie, F., & Chen, C. P. (2025). Adaptive broad network with graph-fuzzy embedding for imbalanced noise data. *IEEE Transactions on Fuzzy Systems*.

Chen, W., Yang, K., Yu, Z., Shi, Y., & Chen, C. P. (2024). A survey on imbalanced learning: latest research, applications and future directions. *Artificial Intelligence Review*, *57*(6), 137.

Chen, L., Yao, Y., & Wang, Z.-l. (2020). Development and validation of a prediction model for the multi-wake of tidal stream turbines. *Renewable Energy*, *155*, 800–809.

Ducange, P., Marcelloni, F., Renda, A., & Ruffini, F. (2025). Fundamentals on explainable and interpretable artificial intelligence models. In *Trustworthy AI in medical imaging* (pp. 279–296). Elsevier.

Ellabban, O., Abu-Rub, H., & Blaabjerg, F. (2014). Renewable energy resources: Current status, future prospects and their enabling technology. *Renewable and Sustainable Energy Reviews*, *39*, 748–764.

Farkas, A., Degiuli, N., Martić, I., Barbarić, M., & Guzović, Z. (2022). The impact of biofilm on marine current turbine performance. *Renewable Energy*, *190*, 584–595.

Fox, C. J., Benjamins, S., Masden, E. A., & Miller, R. (2018). Challenges and opportunities in monitoring the impacts of tidal-stream energy devices on marine vertebrates. *Renewable and Sustainable Energy Reviews*, *81*, 1926–1938.

Gao, L., & Hu, H. (2021). Wind turbine icing characteristics and icing-induced power losses to utility-scale wind turbines. *Proceedings of the National Academy of Sciences*, *118*(42), Article e2111461118.

Goring, D. G., & Nikora, V. I. (2002). Despiking acoustic Doppler velocimeter data. *Journal of Hydraulic Engineering*, *128*(1), 117–126.

Graw, J., Wood, W., & Phrampus, B. (2021). Predicting global marine sediment density using the random forest regressor machine learning algorithm. *Journal of Geophysical Research: Solid Earth*, *126*(1), Article e2020JB020135.

Gunawan, B., Neary, V. S., & Colby, J. (2014). Tidal energy site resource assessment in the East river tidal strait, near Roosevelt Island, New York, New York. *Renewable Energy*, *71*, 509–517.

Habbouche, H., Rashid, H., Amirat, Y., Banerjee, A., & Benbouzid, M. (2024). A 2D VMD video image processing-based transfer learning approach for the detection and estimation of biofouling in tidal stream turbines. *Ocean Engineering*, *312*, Article 119283.

Hanzla, M., & Banerjee, A. (2025). Spectral behavior of a horizontal axis tidal turbine in elevated levels of homogeneous turbulence. *Applied Energy*, *380*, Article 124842.

Harrold, M., & Ouro, P. (2019). Rotor loading characteristics of a full-scale tidal turbine. *Energies*, *12*(6), 1035.

Hong, H., Deng, A., Tang, Y., & Liu, Z. (2024). How to identify biofouling species in marine and freshwater. *Biofouling*, *40*(2), 130–152.

Hong, H., Lv, J., Deng, A., Tang, Y., & Liu, Z. (2024). A review of experimental assessment processes of material resistance to marine and freshwater biofouling. *Journal of Environmental Management*, *357*, Article 120766.

Hosna, T.-B., Haroon, R., & Mohamed, B. (2023). Biofouling issue in tidal stream turbines. In *Design, control and monitoring of tidal stream turbine systems* (pp. 181–204). IET.

Jiang, Y., Zhang, T., Gou, Y., He, L., Bai, H., & Hu, C. (2024). High-resolution temperature and salinity model analysis using support vector regression. *Journal of Ambient Intelligence and Humanized Computing*, 1–9.

Khalid, M., Raza, A., Younas, F., Rustam, F., Villar, M. G., Ashraf, I., & Akhtar, A. (2024). Novel sentiment majority voting classifier and transfer learning-based feature engineering for sentiment analysis of deepfake tweets. *IEEE Access*.

Kishore, P. S. V., Rajesh, J., Jayaram, N., & Halder, S. (2024). A survey of machine learning applications in renewable energy sources. *IETE Journal of Research*, *70*(2), 1389–1406.

Kolekar, N., & Banerjee, A. (2015). Performance characterization and placement of a marine hydrokinetic turbine in a tidal channel under boundary proximity and blockage effects. *Applied Energy*, *148*, 121–133.

Kolekar, N., Vinod, A., & Banerjee, A. (2019). On blockage effects for a tidal turbine in free surface proximity. *Energies*, *12*(17), 3325.

Kong, Q., Zheng, S., Yan, X., Zheng, L., Yang, Y., & Li, Y. (2024). Photoacoustic imaging-based in situ biofouling monitoring in underwater optical windows—A novel approach. *Ocean Engineering*, *309*, Article 118546.

Kyozuka, Y. (2018). Observation of biofouling on two test plates with narrow gap in hirado strait, nagasaki. In *Proceedings of the 2018 IEEE OCEANS - MTS/IEEE kobe techno-oceans* (pp. 1–6). IEEE, http://dx.doi.org/10.1109/OCEANSKOBE.2018.8559066.

Li, C., Liang, B., Yuan, P., Zhang, Q., Tan, J., Si, X., & Liu, Y. (2024). A deep learning approach for hydrofoil optimization of tidal turbines. *Ocean Engineering*, *305*, Article 117996.

Liu, J., Cai, F., Wang, W., Zhu, H., Teng, L., Luo, X., Chen, Y., & Hao, C. (2025). Research on scenario extrapolation and emergency decision-making for fire and explosion accidents at university laboratories based on BN-CBR. *Reliability Engineering & System Safety*, *253*, Article 110579.

Liu, J., Lin, H., Purimitla, S. R., & Mohan Dass, E. (2017). The effects of blade twist and nacelle shape on the performance of horizontal axis tidal current turbines. *Applied Ocean Research*, *64*, 58–69.

Liu, H. w., Ma, S., Li, W., Gu, H.-g., Lin, Y.-g., & Sun, X.-j. (2011). A review on the development of tidal current energy in China. *Renewable and Sustainable Energy Reviews*, *15*(2), 1141–1146.

Malki, R., Williams, A., Croft, T., Togneri, M., & Masters, I. (2013). A coupled blade element momentum–computational fluid dynamics model for evaluating tidal stream turbine performance. *Applied Mathematical Modelling*, *37*(5), 3006–3020.

Mannion, B., Leen, S. B., & Nash, S. (2020). Development and assessment of a blade element momentum theory model for high solidity vertical axis tidal turbines. *Ocean Engineering*, *197*, Article 106918.

Masters, I., Chapman, J., Willis, M., & Orme, J. (2011). A robust blade element momentum theory model for tidal stream turbines including tip and hub loss corrections. *Journal of Marine Engineering & Technology*, *10*(1), 25–35.

Mo, C., Zhu, W., Lu, B., Zu, S., Zhang, F., Chen, J., Zhang, X., Wu, B., Zhang, X., & Huang, J. (2024). Recognition method of turbine pollutant adhesion in tidal stream energy generation systems based on deep learning. *Energy*, Article 131799.

Modali, P. K., Vinod, A., & Banerjee, A. (2021). Towards a better understanding of yawed turbine wake for efficient wake steering in tidal arrays. *Renewable Energy*, *177*, 482–494.

Mohanty, P., Subhadarshini, K., Nayak, R., Pati, U. C., & Mahapatra, K. (2025). Exploring data-driven multivariate statistical models for the prediction of solar energy. In *Computer vision and machine intelligence for renewable energy systems* (pp. 85–101). Elsevier.

Niu, M., Li, Y., Tao, J., Zhou, X., & Schuller, B. W. (2024). DepressionMLP: A multi-layer perceptron architecture for automatic depression level prediction via facial keypoints and action units. *IEEE Transactions on Circuits and Systems for Video Technology*.

Perez, L., Cossu, R., Grinham, A., & Penesis, I. (2022). Tidal turbine performance and loads for various hub heights and wave conditions using high-frequency field measurements and blade element momentum theory. *Renewable Energy*, *200*, 1548–1560.

Pope, S. B. (2000). *Turbulent flows*. Cambridge University Press.

Prexl, J., & Schmitt, M. (2025). Self-supervised learning for multi-modal earth observation data. In *Deep learning for multi-sensor earth observation* (pp. 181–199). Elsevier.

Rashid, H., Benbouzid, M., Amirat, Y., Berghout, T., Titah-Benbouzid, H., & Mamoune, A. (2023). Biofouling detection and extent classification in tidal stream turbines via a soft voting ensemble transfer learning approach. In *IECON 2023- 49th annual conference of the IEEE industrial electronics society* (pp. 01–06). http://dx.doi.org/10.1109/IECON51785.2023.10312201.

Rashid, H., Benbouzid, M., Amirat, Y., Berghout, T., Titah-Benbouzid, H., & Mamoune, A. (2024). Biofouling detection and classification in tidal stream turbines through soft voting ensemble transfer learning of video images. *Engineering Applications of Artificial Intelligence*, *138*, Article 109316.

Rashid, H., Benbouzid, M., Titah-Benbouzid, H., Amirat, Y., Berghout, T., & Mamoune, A. (2023). Mapping a machine learning path forward for tidal stream turbines biofouling detection and estimation. In *IECON 2023- 49th annual conference of the IEEE industrial electronics society* (pp. 1–6). http://dx.doi.org/10.1109/IECON51785.2023.10312077.

Rashid, H., Benbouzid, M., TitahBenbouzid, H., Amirat, Y., & Mamoune, A. (2023). Tidal stream turbine biofouling detection and estimation: A review-based roadmap. *Journal of Marine Science and Engineering*, *11*(5), 908.

Rashid, H., Habbouche, H., Amirat, Y., Mamoune, A., Titah-Benbouzid, H., & Benbouzid, M. (2024). B-FLOWS: Biofouling focused learning and observation for wide-area surveillance in Tidal stream turbines. *Journal of Marine Science and Engineering*, *12*(10), 1828.

Rivier, A., Bennis, A.-C., Jean, G., & Dauvin, J.-C. (2018). Numerical simulations of biofouling effects on the tidal turbine hydrodynamic. *International Marine Energy Journal*, *1*(2 (Nov)), 101–109.

Rotor, M. A., & Hefazi, H. (2022). Shape optimization of a horizontal axis tidal turbine (HATT) blade using neural networks for response surface methodology. In *2022 5th international conference on renewable energy and power engineering* (pp. 302–308). IEEE.

Satrio, D., Musabikha, S., Junianto, S., Prifiharni, S., Kusumastuti, R., Nikitasari, A., & Priyotomo, G. (2024). The advantages and challenges of carbon fiber reinforced polymers for tidal current turbine systems-an overview. *vol. 1298*, In *IOP conference series: earth and environmental science*. IOP Publishing, Article 012029, (1).

Schultz, M., Walker, J., Steppe, C., & Flack, K. (2015). Impact of diatomaceous biofilms on the frictional drag of fouling-release coatings. *Biofouling*, *31*(9–10), 759–773.

Song, S., Demirel, Y. K., Atlar, M., & Shi, W. (2020). Prediction of the fouling penalty on the tidal turbine performance and development of its mitigation measures. *Applied Energy*, *276*, Article 115498.

Starzmann, R., Kaufmann, N., Jeffcoate, P., Pieroway, R., Guerra, M., & Hay, A. (2022). Effect of fouling on the performance of an instream turbine. *International Marine Energy Journal*, *5*(3), 229–237.

Stringer, C. C., & Polagye, B. L. (2020). Implications of biofouling on cross-flow turbine performance. *SN Applied Sciences*, *2*(3), 464.

Thomson, J., Polagye, B., Durgesh, V., & Richmond, M. C. (2012). Measurements of turbulence at two tidal energy sites in puget sound, WA. *IEEE Journal of Oceanic Engineering*, *37*(3), 363–374.

Touimi, K., Benbouzid, M., & Tavner, P. (2018). Tidal stream turbines: With or without a gearbox? *Ocean Engineering*, *170*, 74–88.

Vance, T. R., & Fileman, T. (2014). *ETI MA1001-reliable data acquisition platform for Tidal (ReDAPT) project: ME8.5 final report*: *Tech. rep.*, UK: Energy Technologies Institute.

Vinod, A., & Banerjee, A. (2019). Performance and near-wake characterization of a tidal current turbine in elevated levels of free stream turbulence. *Applied Energy*, *254*, Article 113639.

Vinod, A., Han, C., & Banerjee, A. (2021). Tidal turbine performance and near-wake characteristics in a sheared turbulent inflow. *Renewable Energy*, *175*, 840–852.

Volponi, A. J. (2014). Gas turbine engine health management: past, present, and future trends. *Journal of Engineering for Gas Turbines and Power*, *136*(5), Article 051201.

Walker, J. M., Flack, K. A., Lust, E. E., Schultz, M. P., & Luznik, L. (2014). Experimental and numerical studies of blade roughness and fouling on marine current turbine performance. *Renewable Energy*, *66*, 257–267.

Walker, J., Green, R., Gillies, E., & Phillips, C. (2020). The effect of a barnacle-shaped excrescence on the hydrodynamic performance of a tidal turbine blade section. *Ocean Engineering*, *217*, Article 107849.

Wang, Y., Zhao, H., Deng, R., Tung, F., & Mori, G. (2024). Pretext training algorithms for event sequence data. arXiv preprint arXiv:2402.10392.

Xia, T., Wang, L., Xu, J., Yuan, J., Luo, Z., & Wang, Z. (2024). A novel generative–predictive data-driven approach for multi-objective optimization of horizontal axis tidal turbine. *Physics of Fluids*, *36*(4).

Xu, H., Yang, D., Wang, T., & Benbouzid, M. (2025). Multi-view and multi-type feature fusion rotor biofouling recognition method for tidal stream turbine. *Journal of Marine Science and Engineering*, *13*(2), http://dx.doi.org/10.3390/jmse13020356.

Yang, H., Wu, Q., & Li, G. (2024). A multi-stage forecasting system for daily ocean tidal energy based on secondary decomposition, optimized gate recurrent unit and error correction. *Journal of Cleaner Production*, *449*, Article 141303.

Zhang, Y., Fernandez-Rodriguez, E., Zheng, J., Zheng, Y., Zhang, J., Gu, H., Zang, W., & Lin, X. (2020). A review on numerical development of tidal stream turbine performance and wake prediction. *IEEE Access*, *8*, 79325–79337.

Zhu, J., Su, Z., Wang, Q., Lan, Z., Chan, F. S.-f., Han, Z., Wang, Z., Wong, S. W.-f., & Ngan, A. C.-f. (2024). Surface quality prediction and quantitative evaluation of process parameter effects for 3D printing with transfer learning-enhanced gradient-boosting decision trees. *Expert Systems with Applications*, *237*, Article 121478.